**Disinhibitory circuitry gates associative synaptic plasticity in olfactory cortex**

Martha Canto-Bustos[1,2], F. Kathryn Friason[1,2], Constanza Bassi[1]
and Anne-Marie M. Oswald[1,2,3]*

[1]Department of Neuroscience, [2]Center for the Neural Basis of Cognition,

University of Pittsburgh, Pittsburgh, PA, United States, 15213

**Corresponding Author**:
Anne-Marie M. Oswald
Associate Professor
Department of Neuroscience
University of Pittsburgh
A210 Langley Hall
Pittsburgh, PA, 15260

[3]Current Address
Department of Neurobiology
Neuroscience Institute
University of Chicago
Abbott Memorial Hall
947 East 58th St. MC0928
Chicago, IL, USA, 60637
amoswald@uchicago.edu

**Abstract**

Inhibitory microcircuits play an essential role in regulating cortical responses to sensory stimuli. Interneurons that inhibit dendritic or somatic integration in pyramidal neurons act as gatekeepers for neural activity, synaptic plasticity and the formation of sensory representations. Conversely, interneurons that specifically inhibit other interneurons can open gates through disinhibition. In the rodent piriform cortex, relief of dendritic inhibition permits long-term potentiation (LTP) of the recurrent synapses between pyramidal neurons (PNs) thought to underlie ensemble odor representations. We used an optogenetic approach to identify the inhibitory interneurons and disinhibitory circuits that regulate LTP. We focused on three prominent inhibitory neuron classes- somatostatin (SST), parvalbumin (PV), and vasoactive intestinal polypeptide (VIP) interneurons. We find that LTP is gated by the inactivation SST or PV interneurons or by activation of VIP interneurons. Further, activation of VIP interneurons strongly inhibits putative SST-cells during LTP induction, but only weakly inhibit PV-interneurons. Taken together, these findings suggest that VIP-interneurons mediate a disinhibitory circuit that can regulate synaptic plasticity during olfactory processing.

Throughout the cortex, the response properties of individual neurons as well as coordinated ensemble activity are refined by sensory experience. One underlying feature of experience-dependent plasticity is long-term changes in synaptic strength within cortical circuits. While the mechanisms underlying excitatory synaptic plasticity have been extensively studied (Abbott and Nelson 2000, Malenka and Bear 2004), less is known about the role cortical circuitry plays in gating changes in synaptic strength. Inhibitory interneurons regulate both dendritic integration and neural activity, two major factors in synaptic plasticity. Thus, inhibitory circuits can play a key role in the enhancement of synaptic connections (Artinian and Lacaille 2018, Lucas and Clem 2018). In this study, we elucidate the inhibitory and disinhibitory circuit motifs that gate synaptic plasticity at recurrent excitatory synapses in the olfactory cortex.

The anterior piriform cortex (APC) processes olfactory information, and performs both sensory and associative cortical functions. Located two synapses from the periphery; the APC is a primary cortical area representing odor inputs. Olfactory receptor neurons in the nose project to Mitral and Tufted (M/T) neurons in the olfactory bulb (OB)(Mombaerts, Wang et al. 1996). M/T neurons then project directly to APC and synapse with pyramidal neurons (PNs)(Haberly and Price 1977). Unlike other primary sensory cortices, APC lacks a topological representation of odor identity. M/T axons project diffusely and randomly (Sosulski, Bloom et al. 2011, Igarashi, Ieki et al. 2012) to activate distributed neural ensembles (Illig and Haberly 2003, Rennaker, Chen et al. 2007, Stettler and Axel 2009). Distributed odor representations are further supported by uniform intracortical excitatory connectivity across the APC (Franks, Russo et al. 2011). It is postulated that odor-specific ensembles are constructed by strengthening excitatory synapses between pyramidal neurons co-activated by odor components (Haberly 2001, Wilson and Sullivan 2011). In support of this hypothesis, intracortical synapses between PNs are strengthened following odor learning *in vivo* (Saar, Grossman et al. 2002) and through pairing of afferent and intracortical stimulation *in vitro* (Kanter and Haberly 1993, Johenning, Beed et al. 2009). Hence, APC circuitry also supports early stage, associative odor processing.

53 The APC is an ideal structure for investigating the circuit and synaptic plasticity
54 mechanisms that underlie sensory representations. PNs receive compartmentalized excitatory
55 inputs on their apical dendrites from two distinct fiber tracts. M/T cell afferents synapse distally,
56 while PN axons form a proximal intracortical fiber tract (Haberly and Price 1977, Haberly and
57 Price 1978). Co-activation of afferent and intracortical fiber tracts strengthens intracortical
58 synapses onto PNs through NMDA receptor (R) dependent, associative LTP (Kanter and
59 Haberly 1993). Further, NMDAR EPSPs and associative LTP induction are facilitated by
60 dendritic disinhibition by $GABA_A$ receptor antagonists (Kanter and Haberly 1993, Kanter, Kapur
61 et al. 1996). While these studies suggest interplay between dendritic inhibition and disinhibition
62 gates LTP induction at intracortical synapses, the inhibitory circuitry involved has not been
63 identified.
64 Olfactory stimuli recruit both feedforward and recurrent inhibition onto PNs in APC (Poo
65 and Isaacson 2009, Poo and Isaacson 2011). Feedforward inhibition is comparatively weak and
66 diminishes with high frequency stimulation of the afferent pathway, whereas recurrent inhibition
67 is strong, and increases with stimulation through synaptic facilitation and PN recruitment
68 (Stokes and Isaacson 2010, Suzuki and Bekkers 2010a, Large, Vogler et al. 2016). Recurrent
69 inhibition is mediated by inhibitory interneurons that express somatostatin (SST-INs) or
70 parvalbumin (PV-INs) (Stokes and Isaacson 2010, Suzuki and Bekkers 2010a, Suzuki and
71 Bekkers 2010b, Large, Kunz et al. 2016). SST-INs inhibit PN apical dendrites proximal to the
72 soma, and are optimally located to regulate plasticity of intracortical synapses (Suzuki and
73 Bekkers 2010b, Large, Kunz et al. 2016). PV-INs regulate spike activity and could also impact
74 LTP through backpropagation (Johenning, Beed et al. 2009). A third class of interneurons-
75 vasoactive intestinal polypeptide interneurons (VIP-INs); inhibit SST and PV-INs and could
76 disinhibit pyramidal neurons (Lee, Kruglikov et al. 2013, Pfeffer, Xue et al. 2013, Karnani,
77 Jackson et al. 2016). VIP-INs are a prominent in APC (Suzuki and Bekkers 2010b) but their
78 inhibitory connections and function are unknown. We investigated the connectivity and

79 functional roles of SST, PV and VIP-INs in APC. We find that activation of VIP-INs as well as
80 inactivation of SST-INs or PV-INs promote LTP of intracortical synapses. VIP-INs strongly inhibit
81 SST-INs during LTP induction, but only weakly inhibit PV-INs and PNs. Our finding suggests a
82 VIP->SST>-PN disinhibitory circuit gates associative LTP in APC.
83
84 **Methods:**
85 *Mice:* VIP-Cre (B6:Viptm1(cre)Zjh/J) , SST-Cre (B6:Sst<tm2.1(cre)Zjh>/J) and PV-Cre mice
86 express cre-recombinase (Taniguchi, He et al. 2011). These mice were crossed with Ai32 mice
87 (B6;129S-Gt ROSA)26Sortm32 (CAG-COP4*H134R/EYFP)Hze/J) to express channelrhodopsin
88 (ChR2) or Ai35 mice (B6.129S-*Gt(ROSA*)26Sortm35.1(*CAG- aop3/GFP)Hze*/J) to express
89 archaerhodopsin (Arch) (Madisen, Mao et al. 2012). All mice are from Jackson Laboratory. All
90 animals were bred, handled and treated in manner that was evaluated and approved by the
91 Animal Care and Use Committee at the University of Pittsburgh IACUC, protocol #17070877.
92 *Slice preparation:* APC brain slices were prepared from mice aged P19-35. The mice were
93 anesthetized with isoflurane and the brain was removed and immersed in ice cold oxygenated
94 (95% $O_2$-5% $CO_2$) ACSF (in mM: 125 NaCl, 2.5 KCl, 25 $NaHCO_3$, 1.25 $NaH_2PO_4$, 1.0 $MgCl_2$, 25
95 Glucose, 2.5 $CaCl_2$) (all chemicals from Sigma, USA unless otherwise stated). Parasagittal
96 slices (300 μm) were cut on a vibratome (Leica Biosystems) in ice-cold ACSF. The slices were
97 transferred to warm ACSF (36°C) for 30 min, then 20-22°C for 1 hour, and recorded at 25-28°C.
98 *Electrophysiology*: Recordings were performed using a MultiClamp 700B amplifier (Molecular
99 Devices, Union City, CA). Data were low pass filtered (4 kHz) and digitized at 10 kHz using an
100 ITC-18 (Instrutech) controlled by custom software (Recording Artist,
101 https://bitbucket.org/rgerkin/recording-artist) written in IgorPro (Wavemetrics). Recording
102 pipettes (4-10 MΩ) were pulled from borosilicate glass (1.5 mm, outer diameter) on a
103 Flaming/Brown micropipette puller (Sutter Instruments). The series resistance (<20 MΩ) was not

104 corrected. For PSPs the intracellular solution consisted of (in mM) 130 K-gluconate, 5 KCl, 2
105 $MgCl_2$, 4 ATP-Mg, 0.3 GTP, 10 HEPES, and 10 phosphocreatine, 0.05% biocytin. For IPSC
106 recordings, Qx-314 was added to the K-gluconate internal (holding potential 0 mV) or Cs-Glu-
107 Qx solution was used (in mM, 130 Cs-Gluconate, 5 KCl, 2 $MgCl_2$, 4 Mg-ATP, 0.3 GTP, 10
108 HEPES, 10 Phosphocreatine, 1 Qx-314, holding potential +30 mV). Neurons were visualized
109 using infrared-differential interference contrast microscopy (IR-DIC, Olympus). For all recorded
110 neurons, subthreshold response properties were obtained using a series of hyperpolarizing and
111 depolarizing current steps (-50 pA to 50 pA, 1 s duration). We used specific criteria for
112 identification of putative PV and SST interneurons based on intrinsic properties of identified PV
113 and SST neurons in APC (see (Large, Kunz et al. 2016, for details). Neural identity was
114 confirmed post hoc using intrinsic properties and biocytin fills.
115 *LTP induction:* Electrical stimulation was delivered using concentric bipolar electrodes (FHC).
116 The electrodes were placed in the LOT (L1a) and the L1b/L2 border. Stimuli (100 μs pulse
117 width) were delivered through a stimulus isolation unit. Theta burst stimulation (TBS) of L1a
118 consisted of 10 bursts of 4 pulses (100 Hz) delivered at 250 ms intervals (Kanter and Haberly
119 1993). TBS stimulation intensity was set near spike threshold for the recorded neuron. L1b was
120 stimulated with a single weak pulse delivered between the 3$^{rd}$ and 4$^{th}$ pulse of each burst.
121 Stimulation intensity was <30% of the maximum subthreshold EPSP (~1-6 mV). Pre and post
122 induction test pulses were delivered to L1b every 30 s. Baseline was collected for ~5 min and
123 LTP was induced within 10 min of patching the neuron. Input resistance was monitored
124 throughout and neurons with deviations greater than 20% from baseline were excluded from
125 analysis (n=10 neurons). We also monitored membrane potential throughout recording. Small
126 fluctuations <5 mV were offset with constant current to maintain driving force. However, neurons
127 with drift greater than 5 mV or exhibiting unstable membrane potential fluctuations were
128 excluded from analysis (n=8).

129 *Pharmacology*: The $GABA_A$ receptor antagonist, gabazine (GZ, 20 μM in ACSF) was loaded
130 into a regular patch pipette and focally applied to L1b using a gentle positive pressure (<1-5 s
131 duration) see. Slices were oriented such that bath flowed from the soma to dendrite of the
132 pyramidal cell to maintain GZ in the region of the dendrite. Every effort was made to ensure
133 stability of GZ application including supplemental applications. In a subset of slices (n=5) from
134 mice that expressed ChR2 in SST-INs, GZ application to L1b diminished optically evoked SST-
135 mediated inhibition onto pyramidal cells (n=5). We verified that optically evoked IPSPs (Control:
136 6.3 ± 0.69 mV) in these slices were stably diminished by Gabazine application throughout the
137 LTP protocol and did not differ between baseline (IPSP GZ: 0.89 ± 0.27 mV) and post-induction
138 test pulses (IPSP GZ: 0.92 ± 0.28, p>0.05 WSR). In additional experiments, the NMDA receptor
139 antagonist, DL-2-Amino-5-phosphonopentanoic acid (DL-APV, 10 mM, Sigma-Aldrich) was
140 bath-applied as indicated in the main text.
141 *Optogenetic Stimulation:* Shutter controlled full field stimulation with blue (473 nm) or green
142 (520 nm) light (Prior) was delivered through the epifluorescence pathway of the microscope
143 (Olympus) using a water-immersion objective (40x). Light intensity (5-10 mW) was adjusted to
144 induce spike responses (ChR2 activation) or spike suppression (Arch inactivation). Light pulse
145 duration varied by experiment as indicated in the main text.
146 EPSP Analysis: EPSPs were analyzed using custom software written in IgorPro (Wavemetrics).
147 Because we do not block inhibition during L1b test-pulses, we set narrow criteria to ensure that
148 only the excitatory portion of mixed EPSP-IPSPs was analyzed. Recurrent inhibition is
149 disynaptic and IPSPs are delayed with respect to excitation. Only EPSP onsets within 5 ms of
150 the stimulus artifact were analyzed. Across all conditions the average EPSP onset was 3.7 ±
151 0.41 ms. EPSP peak amplitude was taken as the max amplitude within 5 ms of EPSP onset.
152 We also measured the slope of the rising phase of the EPSP from onset to 80% of peak
153 amplitude to further isolate the EPSP. Our core findings did not differ between peak and slope
154 measurements.

155 Statistics: All data is presented as mean ± SE. Statistical tests were performed using two tailed,
156 one or two-sample, paired or unpaired Student's t-test as appropriate. In cases of small sample
157 sizes non-parametric tests were used, including the Mann-Whitney U-test (MWU) for unpaired
158 data and the Wilcoxon Signed Ranks test (WSR) for paired data. For multiple comparisons we
159 used ANOVA with post hoc Tukey Test (ANOVA).
160
161 **Results:**
162
163 We investigated the roles of SST, PV and VIP-INs, in gating associative LTP at intracortical
164 excitatory synapses onto PNs. Afferent input to PNs arrives via L1a on distal L2 PN dendrites,
165 while the intracortical fiber tract (L1b) is proximal (**Fig 1A**). L1a and L1b were easily identified
166 under IR-DIC and independently stimulated using bipolar electrodes. Associative LTP is induced
167 by pairing L1a and L1b stimulation using a theta burst stimulation (TBS) protocol (Kanter and
168 Haberly 1993) consistent with respiration coupled M/T spike frequencies (Kepecs, Uchida et al.
169 2007, Carey and Wachowiak 2011). Briefly, strong TBS of L1a was paired with weak, single
170 pulse stimulation of L1b (see methods, **Fig 1A**). This L1a+L1b pairing is hereafter denoted
171 *induction*. L1a-TBS evoked low PN firing rates ranging from 0-8 Hz and L1b EPSPs ranged from
172 1-6 mV. Pre and post induction, L1b stimulation was delivered every 30 s. To avoid drift in
173 recording integrity, potentiation was quantified as the average L1b EPSP amplitude 25-30 min
174 following induction versus average baseline EPSP amplitude (5 min prior to induction).
175 However, in neurons where stability could be verified, potentiation typically lasted for the
176 duration of recording (45-60 min). Both raw and normalized (to baseline) EPSP amplitude and
177 rising slope were analyzed. PNs were excluded if input resistance or membrane potential varied
178 from baseline (±20% or ±5 mV respectively).
179
180

181 ***Disinhibition of PN dendrites promotes LTP***

182 With inhibition intact, the induction protocol did not induce LTP of L1b synapses. Neither
183 EPSP amplitude (in mV, pre: 2.6 ± 0.60, post: 2.6 ± 0.51, p: 0.85, paired t-test, n=9) nor slope
184 (in mV/ms, pre: 0.64 ± 0.20, post: 0.61 ± 0.18, p: 0.27, paired t-test, n=9) significantly differed
185 from baseline (pre) at 30 min post induction (**Fig 1B**). Likewise, normalized EPSP amplitude
186 and area did not differ significantly from 1 (Amplitude: 1.0 ± 0.071, p: 0.65; Slope: 0.96 ± 0.079,
187 p: 0.65, one sample t-test, **Fig 1C, D**). However, when we focally applied the $GABA_A$ receptor
188 antagonist, Gabazine (GZ, 20 μM), to L1b (schematic, **Fig 1A**), induction significantly enhanced
189 EPSP amplitude (mV, Pre: 1.3 ± 0.32, Post: 3.1 ± 0.95, p<0.050 WSR, n=6, **Fig 1B**) and slope
190 (mV/ms, Pre: 0.28 ± 0.070, Post: 0.52 ± 0.12, p<0.050 WSR, n=6). Normalized EPSP amplitude
191 and slope were significantly greater than 1 (Amplitude: 2.3 ± 0.35, p<0.05 WSR; Slope: 2.0 ±
192 0.27, p<0.05 WSR, **Fig 1C, D**). Consistent application of dendritic Gabazine for the duration of
193 recording is difficult to maintain. In a some PNs, EPSP amplitudes were potentiated but
194 unstable, these were excluded from analysis (n=5). This highlights the need for a more selective
195 and reliable optogenetic approach to investigating disinhibition.

196 ***Inactivation of SST-INs promotes LTP***

197 We have previously shown that SST-interneurons strongly inhibit PN dendrites in L1B
198 (Large, Kunz et al. 2016). Although SST-INs typically receive weak direct L1a input (Suzuki and
199 Bekkers 2010a), SST-INs are recruited by strong TBS of L1a through the recruitment of
200 recurrent excitation (**Fig 2A1,2).** To investigate the influence of SST-INs on LTP induction,
201 Archaerhodopsin (Arch) was selectively expressed in SST-INs for optical inactivation. During
202 TBS, optical inactivation reduced SST-IN firing rate (FR) from 6.8 ± 1.2 Hz to 1.8 ± 0.4 Hz
203 (p<0.05, WSR test, **Fig 2A2**) and enhanced depolarization in PNs (**Fig 2B**). These findings
204 suggest that SST-interneurons mediate inhibition during TBS stimulation and could prevent
205 associative synaptic plasticity at L1B synapses. To test this, we optically inactivated SST-INs
206 solely during LTP induction (2 sec). EPSP amplitude and slope was significantly enhanced 30

207 min post induction (Amplitude (mV), Pre: 2.6 ± 0.41, Post: 4.3 ± 0.76, p: 0.0071; Slope (mV/ms),
208 Pre: 0.55 ± 0.14, Post: 1.1 ± 0.23, p: 0.0048; n=9, paired t-test, **Fig 2C1,2, E**). Normalized
209 EPSP amplitude and slope were significantly greater than 1 (Amplitude: 1.7 ± 0.16, p: 0.00010;
210 Slope: 2.0 ± 0.24, p: 0.0033, one sample t-test, **Fig 2D**). EPSP traces from representative PNs
211 pre and post induction are shown in **Fig 2E**. The normalized amplitude and slope averaged
212 across neurons over 30 min are shown in **Fig 2F1,2**. To confirm that associative synaptic
213 plasticity was NMDA-receptor dependent, we bath applied the NMDAR antagonist, DL-APV (10
214 mM) to a second set of slices. Antagonism of NMDAR prevented LTP induction despite
215 inactivation of SST-INs. EPSP amplitude and slope 30 min post induction did not significantly
216 differ from baseline (Amplitude (mV): Pre: 4.7 ± 0.81, Post: 4.0 ± 0.73, p: 0.21; Slope (mV/ms),
217 Pre: 0.83 ± 0.19, Post: 0.74 ± 0.18, p: 0.26; n=10, paired t-test, **Fig 2C, black circles)**;
218 (normalized Amplitude: 0.88 ± 0.13, p: 0.38; Slope: 0.85 ± 0.090, p: 0.28, one sample t-test. **Fig**
219 **2D,F black circles**). These findings suggest that inhibition by SST-INs regulates NMDA-
220 dependent associative LTP at L1b intracortical synapses.

221 ***Inactivation of PV-INs promotes LTP***

222 PV-INs strongly inhibit cortical neurons. We investigated whether optogenetic
223 inactivation of PV-INs expressing Arch also promotes associative LTP (**Fig 3A1**). PV-INs are
224 robustly activated during TBS **(Fig 3A2)** and light inactivation significantly decreased FR (Light
225 OFF: 7.2 ± 2.5 Hz, ON: 2.8 ± 1.7 Hz, n=5, p<0.05, WSR, **Fig 3A2, right)**. In a number of PNs,
226 this enhanced EPSP summation **(Fig 3B1**) and/or FR consistent with somatic disinhibition. PV-
227 IN inactivation during induction promoted LTP of EPSP amplitude and slope **(Fig 3C1,C2,**
228 Amplitude (mV), Pre: 1.6 ± 0.34, Post: 2.4 ± 0.40, p: 0.00095; Slope (mV/ms): 0.38 ± 0.10, Post:
229 0.66 ± 0.18, p: 0.016; n=9, paired t-test). Normalized amplitude and slope were significantly >1
230 post induction (Amplitude: 1.6 ± 0.16, p: 0.0063; Slope: 1.8 ± 0.15, p: 0.00061, one sample t-test
231 **Fig 3C3, D**). Antagonism of NMDAR prevented LTP induction mediated by inactivation of PV-
232 INs. EPSP amplitude and slope post induction did not significantly differ from baseline

233 (Amplitude (mV): Pre: 3.3 ± 0.45, Post: 3.0 ± 0.37, p: 0.48; Slope (mV/ms), Pre: 0.44 ± 0.082,
234 Post: 0.52 ± 0.10, p: 0.74; n=8, paired t-test, **Fig 3C, black circles)**; (normalized Amplitude:
235 0.92 ± 0.076, p: 0.65; Slope: 1.0 ± 0.13, p: 0.56, one sample t-test. **Fig 3C,D black circles**).
236 Thus, PV-INs can also regulate the induction of NMDA-dependent associative LTP at L1b
237 intracortical synapses.

238 ***Inhibition of interneurons by VIP-INs***

239 If both SST-IN and PV-INs can inhibit LTP induction, the question remains as to which
240 circuits might provide a means for disinhibition and the promotion of LTP. In other cortices, VIP
241 interneurons inhibit SST-INs and PV-INs (Pfeffer, Xue et al. 2013, Pi, Hangya et al. 2013).
242 Although there are numerous VIP-INs in piriform cortex (Suzuki and Bekkers 2010b), their
243 targets have not been identified. We crossed VIP-cre mice with Ai32 mice to express
244 channelrhodopsin (ChR2) in VIP-INs. We then used light activation to drive single action
245 potentials in VIP-INs while recording potential postsynaptic targets. Typically, VIP-cre mice are
246 crossed with mice that express GFP in SST-INs (GIN-mice) or PV-INs (G42-mice). However,
247 these lines sparsely label SST and PV-INs in APC (Large, Kunz et al. 2016). Instead, we used
248 intrinsic properties to identify putative (p) SST-INs and pPV-INs according criteria determined
249 from recordings in genetically identified SST-INs and PV-INs in APC (Large, Kunz et al.
250 2016)(see methods). Interneurons that could not be confidently identified were excluded from
251 analysis.

252 VIP-INs were activated by brief blue light pulses (5 ms) and IPSCs were recorded in
253 voltage clamp with either Cs-Gluconate-Qx internal (IPSCs, +30 mV) or K-Gluconate-Qx internal
254 (IPSCs, 0 mV). IPSC recordings were most reliable with Cs-Glu-Qx and the data presented (**Fig**
255 **4)** are from this condition**.** VIP-INs inhibited nearly all recorded pSST-INs (86%), most pPV-INs
256 (90%) and PNs (88%). Although high connectivity with SST and PV cells was expected, this
257 was unexpected for PNs (Pfeffer, Xue et al. 2013). VIP-INs strongly inhibited pSST-INs (IPSC
258 amplitude: 303 ± 57 pA, n=19). However, despite a high probability of connection, VIP-INs very

259 weakly inhibited pPV-INs (35 ± 5.8 pA, n=9, p: 0.0008) and PNs (61 ± 14 pA, p: 0.001 n=14,
260 ANOVA, **Fig 4A1**). Qualitatively similar results were found with K-Glu-Qx, however IPSC
261 amplitude and connection probability were considerably lower (% connected, amplitude, #
262 connected: pSST: 73%, 47 ± 14 pA, n=19; pPV: 73%, 31 ± 7.6 pA, n=11; PN: 29%, 21 ± 7.0 pA,
263 n=4).

264 We find that VIP-INs typically show strongly adapting spike responses within the first 500
265 ms of suprathreshold depolarizations by current steps. For this reason, long light pulses (2 s)
266 during LTP induction would likely result in significant adaptation of VIP-INs spike responses.
267 Instead, we drove VIP-INs with shorter light pulses (100 ms) delivered at theta frequency (10
268 pulses, **Fig 4A2**). This pulsed-light stimulation evoked strong and relatively sustained IPSCs in
269 pSST-INs (**Fig 4B2 top**). Overall, IPSC strength decreased by only ~30% by the 5$^{th}$ pulse in all
270 cell types then stabilized (SST: 31 ± 10%, p: 0.002; PV: 31± 5%, p: 0.06; PC: 28 ± 12%, p: 0.02,
271 paired t-test, **Fig 4B2**).

272 To investigate how VIP-IN mediated inhibition could influence action potential activity we
273 depolarized target neurons to near or suprathreshold membrane potentials in current clamp. In
274 pSST-INs activation of VIP-INs evoked strong IPSPs (2.02 ± 0.38 mV, n=18, **Fig 4C1**). These
275 IPSPs were sufficient to delete or delay spikes by an average of 77 ± 26 ms (p: 0.016, n=11,
276 paired t-test) compared to non-light trials (**Fig 4C1,3 left**). Finally, pSST-IN spike responses
277 evoked by TBS were significantly decreased by pulsed activation of VIP-INs compared to non-
278 light trials (OFF: 5.0 ± 0.6 Hz, ON: 3.5 ± 0.5, p: 0.002, n=11, paired t-test, **Fig 4C**). We could not
279 record IPSPs in PNs (n=7) or pPV-INs (n=4) likely due to a combination of low input resistance
280 and weak VIP-mediated IPSCs. Taken together, these findings suggest that VIP-INs could
281 strongly influence pSST-INs during LTP induction but would have considerably less impact on
282 pPV-IN or PNs.
283

284 ***Activation of VIP-INs promotes LTP***

285 VIP-INs are numerous in APC and we find that VIP-INs inhibit pSST-INs. VIP-to-SST
286 inhibition is a candidate circuit motif for dendritic disinhibition of PNs that could promote LTP.
287 So, why isn't LTP induced without antagonism of inhibition? We recorded VIP-INs during TBS
288 stimulation of L1a. We found that in contrast to SST-INs or PV-INs, VIP-INs were only weakly
289 driven to fire action potentials by TBS (0.7 ± 0.6 Hz, n=6, Fig 5A2). This lack of VIP-IN
290 recruitment is consistent with the inability to induce LTP under control conditions (**Fig 1B**).
291 However, light activation of ChR2+ VIP-INs enhanced FR during TBS (14 ± 4.0 Hz, $p<0.05$,
292 WSR test **Fig 5A2**). Activating VIP-INs also enhanced EPSP summation in PNs during TBS
293 **(Fig 5B)**. Activation of VIP-INs during induction lead to robust LTP of EPSP amplitude and slope
294 (**Fig 5C1,C2**, amplitude (mV), Pre: 2.1 ± 0.50, Post: 3.4 ± 0.48, $p<0.02$; slope (mV/ms) Pre: 0.47
295 ± 0.081, Post: 0.76 ± 0.072, $p<0.02$, n=7, WSR). Normalized amplitude and slope were
296 significantly >1 post induction (Amplitude: 2.0 ± 0.33, $p<0.02$; Slope: 1.9 ± 0.32, $p<0.02$, WSR,
297 **Fig 5C3**). Antagonism of NMDARs prevented LTP induction mediated by activation of VIP-INs.
298 EPSP amplitude and slope post induction did not significantly differ from baseline (Amplitude
299 (mV): Pre: 6.0 ± 1.6, Post: 5.5 ± 1.5, $p>0.05$; Slope (mV/ms), Pre: 1.2 ± 0.23, Post: 1.1 ± 0.28,
300 p: >0.05; n=5, WSR, **Fig 5C,D black circles)**; (normalized Amplitude: 0.93 ± 0.072, $p>0.05$;
301 Slope: 0.99 ± 0.17, $p>0.05$, WSR. **Fig 5C,D black circles**). Altogether, these findings support a
302 VIP-SST-PN disinhibitory circuit that gates associative LTP at intracortical synapses.
303

304 **Discussion**

305 It has been hypothesized that odor ensembles are formed through associative plasticity of
306 recurrent excitatory synapses between co-activated pyramidal neurons (Haberly 2001, Wilson
307 and Sullivan 2011). These intracortical synapses are stronger in animals that have learned an
308 olfactory discrimination task (Saar, Grossman et al. 2002, Saar, Reuveni et al. 2012) and the
309 induction of associative LTP *in vitro* is occluded in animals that have learned tasks (Lebel,

310 Grossman et al. 2001). This capacity for enhancement as well as highly recurrent excitation
311 (Poo and Isaacson 2011) necessitates strong inhibition to regulate neural activity (Luna and
312 Schoppa 2008, Poo and Isaacson 2011, Bolding and Franks 2018) and synaptic plasticity
313 (Kanter and Haberly 1993, Kanter, Kapur et al. 1996). Our present findings are consistent with a
314 VIP->SST->PN circuit that transiently disinhibits PN dendrites to promote synaptic plasticity
315 during odor learning while overall inhibition remains intact.

316 Associative LTP at intracortical synapses within APC is well-characterized (Stripling,
317 Patneau et al. 1988, Kanter and Haberly 1993, Poo and Isaacson 2007). TBS provides strong
318 afferent excitation that depolarizes apical PN dendrites and promotes NMDAR dependent
319 potentiation of co-activated intracortical synapses. However, strong TBS also recruits strong
320 inhibition and LTP is rarely induced in the absence of $GABA_AR$ antagonists (Kanter and Haberly
321 1993). We have reproduced previous findings that LTP is gated by dendritic application of
322 Gabazine (Kanter, Kapur et al. 1996, Kumar, Schiff et al. 2018). Further, we have shown that
323 dendritic application of Gabazine blocks inhibition mediated by SST-INs (Large et al., 2016). In
324 the present study, we demonstrate that inactivation of SST-INs at an opportune moment during
325 TBS, is sufficient to promote LTP. Thus, a circuit mechanism that inhibits SST-INs during LTP
326 induction could gate synaptic plasticity. Throughout the cortex, VIP-INs inhibit SST-INs and
327 potentially disinhibit PNs (Lee, Kruglikov et al. 2013, Pfeffer, Xue et al. 2013, Karnani, Jackson
328 et al. 2016). We show that VIP-INs strongly inhibit pSST-INs and weakly inhibit pPV-INs as well
329 as PNs. Moreover, optogenetic activation of VIP-INs decreases pSST-IN spike responses
330 during TBS. Finally, activation of VIP-INs specifically during TBS is sufficient gate associative
331 LTP. Based on these findings, we propose that a VIP->SST->PN disinhibitory circuit gates
332 intracortical synaptic plasticity in APC.

333 However, it is relevant to discuss three additional circuits that are potentially recruited
334 with VIP-IN activation. For example, VIP-INs could also gate plasticity through a VIP-PV-PN
335 disinhibitory circuit. Although optogenetic inactivation of PV-INs promotes LTP, we predict this

336 circuit motif contributes minimally to associative LTP induction. VIP-INs very weakly inhibit
337 pPV-INs, which is likely insufficient to prevent PV-IN spiking during TBS. Conversely, SST-INs
338 strongly inhibit PV-INs (Pfeffer, Xue et al. 2013, Xu, Jeong et al. 2013, Large, Kunz et al. 2016)
339 and inactivation of SST-INs in APC increases pPV-IN activity (Sturgill and Isaacson, 2015).
340 Instead of disinhibiting the PN, a VIP-SST-PV circuit could transiently increase somatic PV-IN
341 inhibition to compensate for a loss of SST mediated inhibition at the dendrite and/or soma.
342 Finally, VIP-INs also inhibit PNs directly, possibly through basket like synapses on the soma
343 (Suzuki and Bekkers 2010a). As with VIP-PV synapses, this VIP-PN inhibitory circuit is also
344 weak and its role is unknown. Importantly, recruitment of these additional circuits does not
345 impair LTP induction with VIP-IN activation. Rather, the interplay of these circuits suggests a
346 shift in inhibition from the dendrite to soma that may stabilize neural responses while opening a
347 window for plasticity.

348 Our study complements a recent study in somatosensory cortex that used
349 chemogenetics to inhibit VIP-INs or SST-INs and prevent or promote LTP induction respectively
350 (Williams and Holtmaat 2019). Together, these two studies support a common VIP->SST->PN
351 disinhibitory circuit motif regulates synaptic plasticity across cortical areas. A benefit of the
352 present study is that by using optogenetics, we were ability to isolate the influence of
353 disinhibition to a brief time window (~2 s) when afferent and intracortical pathways are co-
354 activated. This suggests that transient dendritic disinhibition is sufficient to gate the cascade of
355 intracellular mechanisms underlying synaptic enhancement. Thus, circuit mechanisms that
356 provide a means for VIP cells to be activated in conjunction with odor sampling could play a key
357 role in odor learning and ensemble formation.

358 Interestingly, VIP-INs are not recruited by pairing afferent and intracortical stimulation,
359 this may underlie the inability induce associative LTP with inhibition intact (**Fig 1**). At present, it
360 is not known how VIP-INs in APC are recruited. In other cortices, VIP-IN activity is enhanced by
361 arousal, locomotion, task engagement or reward (Lee, Kruglikov et al. 2013, Pi, Hangya et al.

362 2013, Fu, Tucciarone et al. 2014, Jackson, Ayzenshtat et al. 2016), either through additional
363 excitatory drive from other cortical areas (Lee, Kruglikov et al. 2013, Williams and Holtmaat
364 2019) or through neuromodulation (Porter, Cauli et al. 1999, Lee, Hjerling-Leffler et al. 2010,
365 Alitto and Dan 2012, Kuchibhotla, Gill et al. 2017, Pronneke, Witte et al. 2019). Direct excitatory
366 inputs to VIP-INs would have to be well-timed with respect to sensory stimulation. Conversely,
367 neuromodulation could raise the excitability of VIP-INs such that afferent and intracortical drive
368 are sufficient to drive VIP-INs with appropriate timing. The APC receives input from higher
369 cortices including orbitofrontal cortex (Illig 2005) as well as neuromodulatory centers
370 (Zaborszky, Carlsen et al. 1986, Linster, Wyble et al. 1999). Both of these pathways have been
371 implicated in olfactory learning and plasticity (Patil, Linster et al. 1998, Patil and Hasselmo 1999,
372 Linster, Maloney et al. 2003, Li, Luxenberg et al. 2006, Chapuis and Wilson 2013, Cohen,
373 Wilson et al. 2015, Strauch and Manahan-Vaughan 2018). Future studies are needed to
374 ascertain the potential links between descending excitation and/or neuromodulation, the
375 recruitment of VIP-INs, and the gating of synaptic plasticity during olfactory processing.
376 Though many previous studies have focused on the influence of disinhibitory circuits on
377 FR or behavior, our study highlights a role for disinhibition in the dynamics that gate long-term
378 plasticity. Specifically, our findings suggest that the VIP-SST-PN circuit motif plays a central role
379 in gating synaptic plasticity in PN dendrites. Additional circuit mechanisms mediated through
380 VIP-INs that regulate PV-INs or PNs directly could serve a stabilizing role. These findings
381 demonstrate the challenge of the delineating roles for the individual circuit motifs that are nested
382 in complex neural networks. It remains to be determined if these mechanisms work in concert
383 during afferent and recurrent olfactory processing.
384
385
386
387

388 **Figure 1: Associative LTP of intracortical synapses is gated by dendritic disinhibition.**
389 **A)** Schematic of APC circuit and stimulation paradigm. Strong (s) TBS of afferents (L1a) is
390 paired with weak (w) single-pulses at the intracortical pathway (L1b). Gabazine (GZ) is focally
391 applied to the dendrite region in L1b (tan oval). **B1)** Representative average traces pre (gray)
392 and post induction in control (black) and with GZ(Tan). **B2)** Average EPSP amplitude (mV) pre
393 (-5 to 0 min) and post induction (25-30 min) with inhibition intact (black) or with dendritic GZ
394 (tan). **B3)** Average slope (mV/ms) of the 20-80% rising phase of the EPSP pre and post
395 induction. **C1)** Time course of normalized EPSP amplitude pre and post induction (grey box,
396 t=0) in control (black) and with dendritic Gabazine (tan). **C2)** Time course of normalized EPSP
397 slope, colors as in C2. **C3)** Normalized EPSP amplitude, and slope 30 min post induction in
398 control (black) and with GZ (tan).
399
400 **Figure 2: SST-interneuron inactivation promotes associative LTP. A1)** Schematic: SST-
401 INs express Archaerhodopsin (Arch). **A2)** SST-IN spike responses during TBS in control (black)
402 and inactivated (green) conditions (*$p<0.05$, WSR test). **B)** PN responses for a single TBS
403 burst. **Left :** Inactivation of SST-INs enhanced PN depolarization (green vs. black trace).
404 **Right:** Depolarization during SST-IN inactivation (green) is reduced by APV (gray trace). **C1)**
405 Average EPSP amplitude (mV) pre (-5 to 0 min) and post induction (25-30 min) with SST-
406 inactivation (Magenta) or with SST-inactivation plus bath application of the NMDAR antagonist,
407 APV (black). **C2)** Average slope (mV/ms) of the 20-80% rising phase of the EPSP pre and post
408 induction, colors as in B2. **C3)** Normalized EPSP amplitude and slope following pairing with
409 SST-IN inactivation (magenta circles). LTP is blocked by bath application APV (black). **D1)**
410 Representative average traces pre (gray) and post induction in with SST-IN inactivation
411 (magenta) or inactivation plus APV (Black). **D2)** Time course of normalized EPSP amplitude pre
412 and post induction with inactivation of SST-INs (green box, t=0) in control (magenta) and with
413 bath application of APV (black). **D3)** Time course of normalized EPSP slope, colors as in D2.

414 **Figure 3: PV-interneuron inactivation during induction promotes associative LTP. A1)**
415 Schematic: PV-INs express Archaerhodopsin (Arch). **A2)** PV-IN spike responses during TBS in
416 control (black) and inactivated (green) conditions. **B)** Representative PN responses for a single
417 TBS for control (black) versus PV-IN inactivation (green). **C1)** Average EPSP amplitude (mV)
418 pre (-5 to 0 min) and post induction (25-30 min) with PV-inactivation (Blue) or with PV-
419 inactivation plus bath application of the NMDAR antagonist, APV (black). **C2)** Average slope
420 (mV/ms) of the 20-80% rising phase of the EPSP pre and post induction, colors as in B2. **C3)**
421 Normalized EPSP amplitude and slope following pairing with PV-IN inactivation (blue circles) or
422 with inactivation plus bath application APV (black). **D1)** Representative average traces pre
423 (gray) and post induction in with PV-IN inactivation (blue) or inactivation plus APV (Black). **D2)**
424 Time course of normalized EPSP amplitude pre and post induction with inactivation of PV-INs
425 (green box, t=0) in control (blue) and with bath application of APV (black). **D3)** Time course of
426 normalized EPSP slope, colors as in D2.
427
428 **Figure 4: Inhibition by VIP-interneurons in piriform cortex. A1)** VIP-INs express ChR2.
429 Optically evoked IPSCs were recorded in putative(p) pSST-INs (magenta), pPV-INs (blue) and
430 PNs (black). **A2)** IPSCs recorded in response to ten light pulses (100 ms duration, 4 Hz, same
431 neurons as in A1). **B1)** IPSC amplitudes were stronger in pSST-INs versus pPV-INs (*p:0.014)
432 or PNs (*p:0.042, ANOVA). **B2**) In pSST-INs, IPSC amplitude diminishes by the $5^{th}$ pulse of
433 theta stimulation (**p: 0.009, paired t-test). **C1)** IPSCs from VIP-INs delay pSST-IN spike
434 responses during suprathreshold depolarization (4 overlaid traces) **Left:** Control, **Right**:
435 activation of VIP-INs (100 ms pulse, blue). Magenta trace: VIP-IN mediated IPSC during
436 subthreshold depolarization. **C2)** Interspike interval (ISI) was significantly increased during
437 optical activation of VIP-INs (blue circles, p: 0.016, paired t-test, n=11) compared to light off
438 trials (black circles). **D1)** Spike responses in pSST-INs during TBS in control (magenta trace)

439 and during pulsed light (blue trace). **D2**) pSST-IN firing rates decreased during TBS on light
440 trials (blue) versus control (black circles, p:0.002, paired t-test, n=11).
441
442 **Figure 5: VIP-interneuron activation promotes associative LTP. A1)** Circuit schematic: VIP-
443 INs express ChR2 and were activated using theta pulsed light during L1a+L1b pairing. **A2)** VIP-
444 IN responses during TBS without (black) and with light (blue). FRs increase during pairing with
445 light (blue circles, $p<0.05$, WSR, n=7). **B)** Top: Activation of VIP-INs enhanced PN
446 depolarization during TBS stimulation (blue vs. black trace). Bottom: PN depolarization during
447 VIP-IN activation (blue trace) is reduced by APV (gray trace). **C1)** Average EPSP amplitude
448 (mV) pre (-5 to 0 min) and post induction (25-30 min) with VIP-IN activation (green) or with VIP-
449 IN activation plus bath application of APV (black). **C2)** Average slope (mV/ms) of the rising
450 phase of the EPSP pre and post induction, colors as in C1. **C3)** Normalized EPSP amplitude
451 and slope following pairing with VIP-IN activation (green circles) or with activation plus APV
452 (black). **D1)** Representative average traces pre (gray) and post induction with VIP-IN activation
453 (green) or activation plus APV (Black). **D2)** Time course of normalized EPSP amplitude pre and
454 post induction with activation of VIP-INs (blue box, t=0) in control (green) and with APV (black).
455 **D3)** Time course of normalized EPSP slope, colors as in D2.
456
457
458
459
460
461
462
463
464

465 **References**


466 Abbott, L. F. and S. B. Nelson (2000). "Synaptic plasticity: taming the beast." Nat Neurosci **3**
467 **Suppl**: 1178-1183.
468 Alitto, H. J. and Y. Dan (2012). "Cell-type-specific modulation of neocortical activity by basal
469 forebrain input." Front Syst Neurosci **6**: 79.
470 Artinian, J. and J. C. Lacaille (2018). "Disinhibition in learning and memory circuits: New
471 vistas for somatostatin interneurons and long-term synaptic plasticity." Brain Res Bull **141**:
472 20-26.
473 Bathellier, B., T. W. Margrie and M. E. Larkum (2009). "Properties of piriform cortex
474 pyramidal cell dendrites: implications for olfactory circuit design." J Neurosci **29**(40):
475 12641-12652.
476 Bolding, K. A. and K. M. Franks (2018). "Recurrent cortical circuits implement
477 concentration-invariant odor coding." Science **361**(6407).
478 Carey, R. M. and M. Wachowiak (2011). "Effect of sniffing on the temporal structure of
479 mitral/tufted cell output from the olfactory bulb." J Neurosci **31**(29): 10615-10626.
480 Chapuis, J. and D. A. Wilson (2013). "Cholinergic modulation of olfactory pattern
481 separation." Neurosci Lett **545**: 50-53.
482 Cohen, Y., D. A. Wilson and E. Barkai (2015). "Differential modifications of synaptic weights
483 during odor rule learning: dynamics of interaction between the piriform cortex with lower
484 and higher brain areas." Cereb Cortex **25**(1): 180-191.
485 Franks, K. M., M. J. Russo, D. L. Sosulski, A. A. Mulligan, S. A. Siegelbaum and R. Axel (2011).
486 "Recurrent circuitry dynamically shapes the activation of piriform cortex." Neuron **72**(1):
487 49-56.
488 Fu, Y., J. M. Tucciarone, J. S. Espinosa, N. Sheng, D. P. Darcy, R. A. Nicoll, Z. J. Huang and M. P.
489 Stryker (2014). "A cortical circuit for gain control by behavioral state." Cell **156**(6): 1139-
490 1152.
491 Haberly, L. B. (2001). "Parallel-distributed processing in olfactory cortex: new insights
492 from morphological and physiological analysis of neuronal circuitry." Chem Senses **26**(5):
493 551-576.

494 Haberly, L. B. and J. L. Price (1977). "The axonal projection patterns of the mitral and tufted
495 cells of the olfactory bulb in the rat." Brain Res **129**(1): 152-157.
496 Haberly, L. B. and J. L. Price (1978). "Association and commissural fiber systems of the
497 olfactory cortex of the rat. II. Systems originating in the olfactory peduncle." J Comp Neurol
498 **181**(4): 781-807.
499 Igarashi, K. M., N. Ieki, M. An, Y. Yamaguchi, S. Nagayama, K. Kobayakawa, R. Kobayakawa,
500 M. Tanifuji, H. Sakano, W. R. Chen and K. Mori (2012). "Parallel mitral and tufted cell
501 pathways route distinct odor information to different targets in the olfactory cortex." J
502 Neurosci **32**(23): 7970-7985.
503 Illig, K. R. (2005). "Projections from orbitofrontal cortex to anterior piriform cortex in the
504 rat suggest a role in olfactory information processing." J Comp Neurol **488**(2): 224-231.
505 Illig, K. R. and L. B. Haberly (2003). "Odor-evoked activity is spatially distributed in
506 piriform cortex." J Comp Neurol **457**(4): 361-373.
507 Jackson, J., I. Ayzenshtat, M. M. Karnani and R. Yuste (2016). "VIP+ interneurons control
508 neocortical activity across brain states." J Neurophysiol **115**(6): 3008-3017.
509 Johenning, F. W., P. S. Beed, T. Trimbuch, M. H. Bendels, J. Winterer and D. Schmitz (2009).
510 "Dendritic compartment and neuronal output mode determine pathway-specific long-term
511 potentiation in the piriform cortex." The Journal of Neuroscience **29**(43): 13649-13661.
512 Kanter, E. D. and L. B. Haberly (1993). "Associative long-term potentiation in piriform
513 cortex slices requires GABAA blockade." J Neurosci **13**(6): 2477-2482.
514 Kanter, E. D., A. Kapur and L. B. Haberly (1996). "A dendritic GABAA-mediated IPSP
515 regulates facilitation of NMDA-mediated responses to burst stimulation of afferent fibers in
516 piriform cortex." J Neurosci **16**(1): 307-312.
517 Karnani, M. M., J. Jackson, I. Ayzenshtat, A. Hamzehei Sichani, K. Manoocheri, S. Kim and R.
518 Yuste (2016). "Opening Holes in the Blanket of Inhibition: Localized Lateral Disinhibition
519 by VIP Interneurons." J Neurosci **36**(12): 3471-3480.
520 Kepecs, A., N. Uchida and Z. F. Mainen (2007). "Rapid and precise control of sniffing during
521 olfactory discrimination in rats." J Neurophysiol **98**(1): 205-213.
522 Kuchibhotla, K. V., J. V. Gill, G. W. Lindsay, E. S. Papadoyannis, R. E. Field, T. A. Sten, K. D.
523 Miller and R. C. Froemke (2017). "Parallel processing by cortical inhibition enables context-
524 dependent behavior." Nat Neurosci **20**(1): 62-71.

525 Kumar, A., O. Schiff, E. Barkai, B. W. Mel, A. Poleg-Polsky and J. Schiller (2018). "NMDA
526 spikes mediate amplification of inputs in the rat piriform cortex." Elife **7**.
527 Large, A. M., N. A. Kunz, S. L. Mielo and A. M. Oswald (2016). "Inhibition by Somatostatin
528 Interneurons in Olfactory Cortex." Front Neural Circuits **10**: 62.
529 Large, A. M., N. W. Vogler, S. Mielo and A. M. Oswald (2016). "Balanced feedforward
530 inhibition and dominant recurrent inhibition in olfactory cortex." Proc Natl Acad Sci U S A
531 **113**(8): 2276-2281.
532 Lebel, D., Y. Grossman and E. Barkai (2001). "Olfactory learning modifies predisposition for
533 long-term potentiation and long-term depression induction in the rat piriform (olfactory)
534 cortex." Cereb Cortex **11**(6): 485-489.
535 Lee, S., J. Hjerling-Leffler, E. Zagha, G. Fishell and B. Rudy (2010). "The largest group of
536 superficial neocortical GABAergic interneurons expresses ionotropic serotonin receptors."
537 The Journal of Neuroscience **30**(50): 16796-16808.
538 Lee, S., I. Kruglikov, Z. J. Huang, G. Fishell and B. Rudy (2013). "A disinhibitory circuit
539 mediates motor integration in the somatosensory cortex." Nat Neurosci **16**(11): 1662-
540 1670.
541 Li, W., E. Luxenberg, T. Parrish and J. A. Gottfried (2006). "Learning to smell the roses:
542 experience-dependent neural plasticity in human piriform and orbitofrontal cortices."
543 Neuron **52**(6): 1097-1108.
544 Linster, C., M. Maloney, M. Patil and M. E. Hasselmo (2003). "Enhanced cholinergic
545 suppression of previously strengthened synapses enables the formation of self-organized
546 representations in olfactory cortex." Neurobiol Learn Mem **80**(3): 302-314.
547 Linster, C., B. P. Wyble and M. E. Hasselmo (1999). "Electrical stimulation of the horizontal
548 limb of the diagonal band of broca modulates population EPSPs in piriform cortex." J
549 Neurophysiol **81**(6): 2737-2742.
550 Lucas, E. K. and R. L. Clem (2018). "GABAergic interneurons: The orchestra or the
551 conductor in fear learning and memory?" Brain Res Bull **141**: 13-19.
552 Luna, V. M. and N. E. Schoppa (2008). "GABAergic circuits control input-spike coupling in
553 the piriform cortex." J Neurosci **28**(35): 8851-8859.
554 Madisen, L., T. Mao, H. Koch, J. M. Zhuo, A. Berenyi, S. Fujisawa, Y. W. Hsu, A. J. Garcia, 3rd, X.
555 Gu, S. Zanella, J. Kidney, H. Gu, Y. Mao, B. M. Hooks, E. S. Boyden, G. Buzsaki, J. M. Ramirez, A.

556 R. Jones, K. Svoboda, X. Han, E. E. Turner and H. Zeng (2012). "A toolbox of Cre-dependent
557 optogenetic transgenic mice for light-induced activation and silencing." Nat Neurosci
558 **15**(5): 793-802.
559 Malenka, R. C. and M. F. Bear (2004). "LTP and LTD: an embarrassment of riches." Neuron
560 **44**(1): 5-21.
561 Mombaerts, P., F. Wang, C. Dulac, S. K. Chao, A. Nemes, M. Mendelsohn, J. Edmondson and R.
562 Axel (1996). "Visualizing an olfactory sensory map." Cell **87**(4): 675-686.
563 Patil, M. M. and M. E. Hasselmo (1999). "Modulation of inhibitory synaptic potentials in the
564 piriform cortex." J Neurophysiol **81**(5): 2103-2118.
565 Patil, M. M., C. Linster, E. Lubenov and M. E. Hasselmo (1998). "Cholinergic agonist
566 carbachol enables associative long-term potentiation in piriform cortex slices." J
567 Neurophysiol **80**(5): 2467-2474.
568 Pfeffer, C. K., M. Xue, M. He, Z. J. Huang and M. Scanziani (2013). "Inhibition of inhibition in
569 visual cortex: the logic of connections between molecularly distinct interneurons." Nat
570 Neurosci **16**(8): 1068-1076.
571 Pi, H. J., B. Hangya, D. Kvitsiani, J. I. Sanders, Z. J. Huang and A. Kepecs (2013). "Cortical
572 interneurons that specialize in disinhibitory control." Nature **503**(7477): 521-524.
573 Poo, C. and J. S. Isaacson (2007). "An early critical period for long-term plasticity and
574 structural modification of sensory synapses in olfactory cortex." J Neurosci **27**(28): 7553-
575 7558.
576 Poo, C. and J. S. Isaacson (2009). "Odor representations in olfactory cortex: "sparse" coding,
577 global inhibition, and oscillations." Neuron **62**(6): 850-861.
578 Poo, C. and J. S. Isaacson (2011). "A major role for intracortical circuits in the strength and
579 tuning of odor-evoked excitation in olfactory cortex." Neuron **72**(1): 41-48.
580 Porter, J. T., B. Cauli, K. Tsuzuki, B. Lambolez, J. Rossier and E. Audinat (1999). "Selective
581 excitation of subtypes of neocortical interneurons by nicotinic receptors." The Journal of
582 Neuroscience **19**(13): 5228-5235.
583 Pronneke, A., M. Witte, M. Mock and J. F. Staiger (2019). "Neuromodulation Leads to a
584 Burst-Tonic Switch in a Subset of VIP Neurons in Mouse Primary Somatosensory (Barrel)
585 Cortex." Cereb Cortex.

586 Rennaker, R. L., C. F. Chen, A. M. Ruyle, A. M. Sloan and D. A. Wilson (2007). "Spatial and
587 temporal distribution of odorant-evoked activity in the piriform cortex." J Neurosci **27**(7):
588 1534-1542.
589 Saar, D., Y. Grossman and E. Barkai (2002). "Learning-induced enhancement of
590 postsynaptic potentials in pyramidal neurons." J Neurophysiol **87**(5): 2358-2363.
591 Saar, D., I. Reuveni and E. Barkai (2012). "Mechanisms underlying rule learning-induced
592 enhancement of excitatory and inhibitory synaptic transmission." J Neurophysiol **107**(4):
593 1222-1229.
594 Sosulski, D. L., M. L. Bloom, T. Cutforth, R. Axel and S. R. Datta (2011). "Distinct
595 representations of olfactory information in different cortical centres." Nature **472**(7342):
596 213-216.
597 Stettler, D. D. and R. Axel (2009). "Representations of odor in the piriform cortex." Neuron
598 **63**(6): 854-864.
599 Stokes, C. C. and J. S. Isaacson (2010). "From dendrite to soma: dynamic routing of
600 inhibition by complementary interneuron microcircuits in olfactory cortex." Neuron **67**(3):
601 452-465.
602 Strauch, C. and D. Manahan-Vaughan (2018). "In the Piriform Cortex, the Primary Impetus
603 for Information Encoding through Synaptic Plasticity Is Provided by Descending Rather
604 than Ascending Olfactory Inputs." Cereb Cortex **28**(2): 764-776.
605 Stripling, J. S., D. K. Patneau and C. A. Gramlich (1988). "Selective long-term potentiation in
606 the pyriform cortex." Brain Res **441**(1-2): 281-291.
607 Sturgill, J. F. and J. S. Isaacson (2015). "Somatostatin cells regulate sensory response fidelity
608 via subtractive inhibition in olfactory cortex." Nat Neurosci **18**(4): 531-535.
609 Suzuki, N. and J. M. Bekkers (2010a). "Distinctive classes of GABAergic interneurons
610 provide layer-specific phasic inhibition in the anterior piriform cortex." Cereb Cortex
611 **20**(12): 2971-2984.
612 Suzuki, N. and J. M. Bekkers (2010b). "Inhibitory neurons in the anterior piriform cortex of
613 the mouse: classification using molecular markers." J Comp Neurol **518**(10): 1670-1687.
614 Taniguchi, H., M. He, P. Wu, S. Kim, R. Paik, K. Sugino, D. Kvitsiani, Y. Fu, J. Lu, Y. Lin, G.
615 Miyoshi, Y. Shima, G. Fishell, S. B. Nelson and Z. J. Huang (2011). "A resource of Cre driver

lines for genetic targeting of GABAergic neurons in cerebral cortex." Neuron **71**(6): 995-1013.

Williams, L. E. and A. Holtmaat (2019). "Higher-Order Thalamocortical Inputs Gate Synaptic Long-Term Potentiation via Disinhibition." Neuron **101**(1): 91-102 e104.

Wilson, D. A. and R. M. Sullivan (2011). "Cortical processing of odor objects." Neuron **72**(4): 506-519.

Xu, H., H. Y. Jeong, R. Tremblay and B. Rudy (2013). "Neocortical somatostatin-expressing GABAergic interneurons disinhibit the thalamorecipient layer 4." Neuron **77**(1): 155-167.

Zaborszky, L., J. Carlsen, H. R. Brashear and L. Heimer (1986). "Cholinergic and GABAergic afferents to the olfactory bulb in the rat with special emphasis on the projection neurons in the nucleus of the horizontal limb of the diagonal band." J Comp Neurol **243**(4): 488-509.

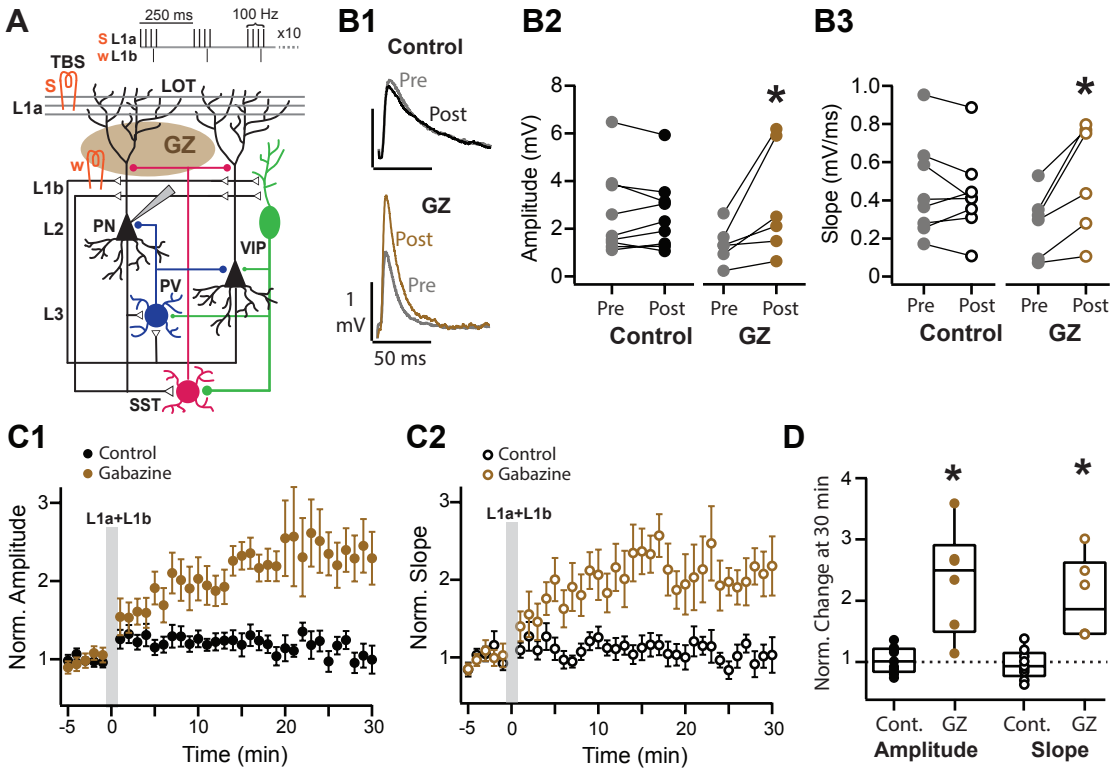


**Figure 1: Associative LTP of intracortical synapses is gated by dendritic disinhibition.** A) Schematic of APC circuit and stimulation paradigm. Strong (s) TBS of afferents (L1a) is paired with weak (w) single-pulses at the intracortical pathway (L1b). Gabazine (GZ) is focally applied to the dendrite region in L1b (tan oval). B1) Representative average traces pre (gray) and post induction in control (black) and with GZ(Tan). B2) Average EPSP amplitude (mV) pre (-5 to 0 min) and post induction (25-30 min) with inhibition intact (black) or with dendritic GZ (tan). B3) Average slope (mV/ms) of the 20-80% rising phase of the EPSP pre and post induction. C1) Time course of normalized EPSP amplitude pre and post induction (grey box, t=0) in control (black) and with dendritic Gabazine (tan). C2) Time course of normalized EPSP slope, colors as in C2. C3) Normalized EPSP amplitude, and slope 30 min post induction in control (black) and with GZ (tan).

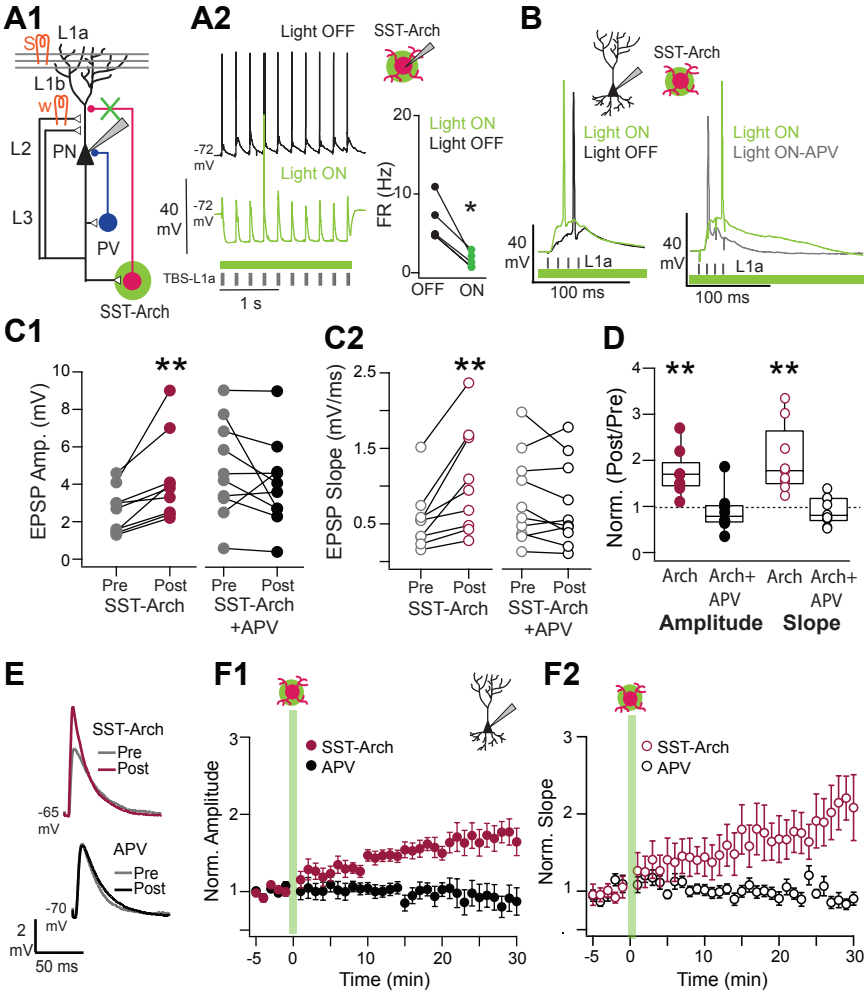


**Figure 2: SST-interneuron inactivation promotes associative LTP.** A1) Schematic: SST-INs express Archaerhodopsin (Arch). A2) SST-IN spike responses during TBS in control (black) and inactivated (green) conditions (*p<0.05, WSR test). B) PN responses for a single TBS burst. Left : Inactivation of SST-INs enhanced PN depolarization (green vs. black trace). Right: Depolarization during SST-IN inactivation (green) is reduced by APV (gray trace). C1) Average EPSP amplitude (mV) pre (-5 to 0 min) and post induction (25-30 min) with SST-inactivation (Magenta) or with SST-inactivation plus bath application of the NMDAR antagonist, APV (black). C2) Average slope (mV/ms) of the 20-80% rising phase of the EPSP pre and post induction, colors as in B2. C3) Normalized EPSP amplitude and slope following pairing with SST-IN inactivation (magenta circles). LTP is blocked by bath application APV (black). D1) Representative average traces pre (gray) and post induction in with SST-IN inactivation (magenta) or inactivation plus APV (Black). D2) Time course of normalized EPSP amplitude pre and post induction with inactivation of SST-INs (green box, t=0) in control (magenta) and with bath application of APV (black). D3) Time course of normalized EPSP slope, colors as in D2.

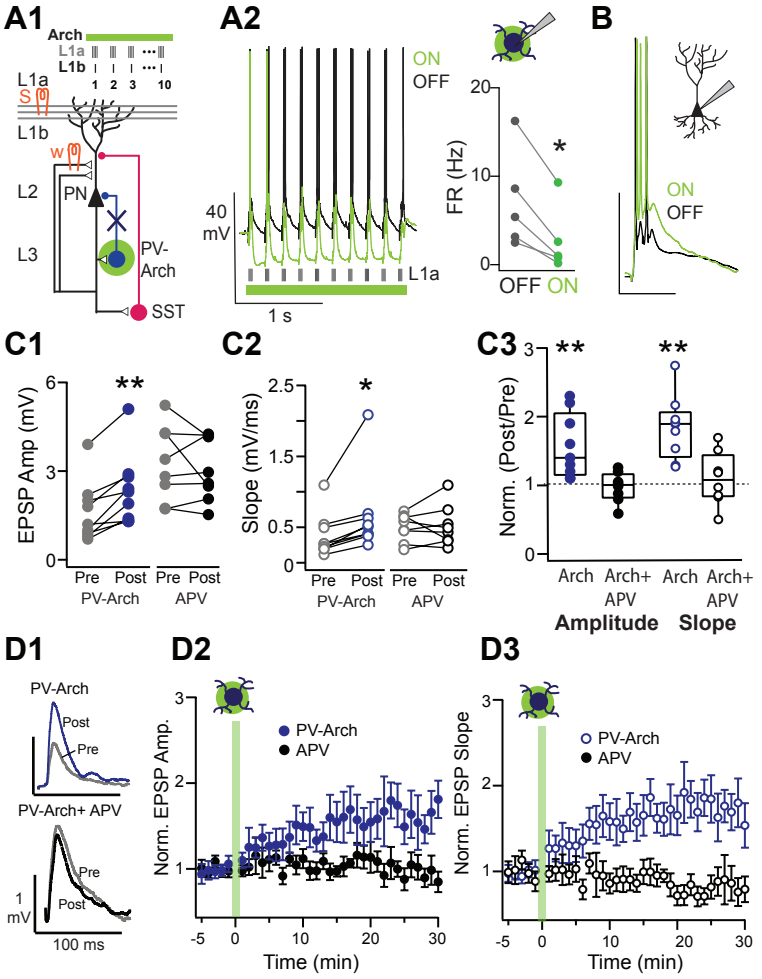


**Figure 3: PV-interneuron inactivation during induction promotes associative LTP.** A1) Schematic: PV-INs express Archaerhodopsin (Arch). A2) PV-IN spike responses during TBS in control (black) and inactivated (green) conditions. B) Representative PN responses for a single TBS for control (black) versus PV-IN inactivation (green). C1) Average EPSP amplitude (mV) pre (-5 to 0 min) and post induction (25-30 min) with PV-inactivation (Blue) or with PV-inactivation plus bath application of the NMDAR antagonist, APV (black). C2) Average slope (mV/ms) of the 20-80% rising phase of the EPSP pre and post induction, colors as in B2. C3) Normalized EPSP amplitude and slope following pairing with PV-IN inactivation (blue circles) or with inactivation plus bath application APV (black). D1) Representative average traces pre (gray) and post induction in with PV-IN inactivation (blue) or inactivation plus APV (Black). D2) Time course of normalized EPSP amplitude pre and post induction with inactivation of PV-INs (green box, t=0) in control (blue) and with bath application of APV (black). D3) Time course of normalized EPSP slope, colors as in D2.

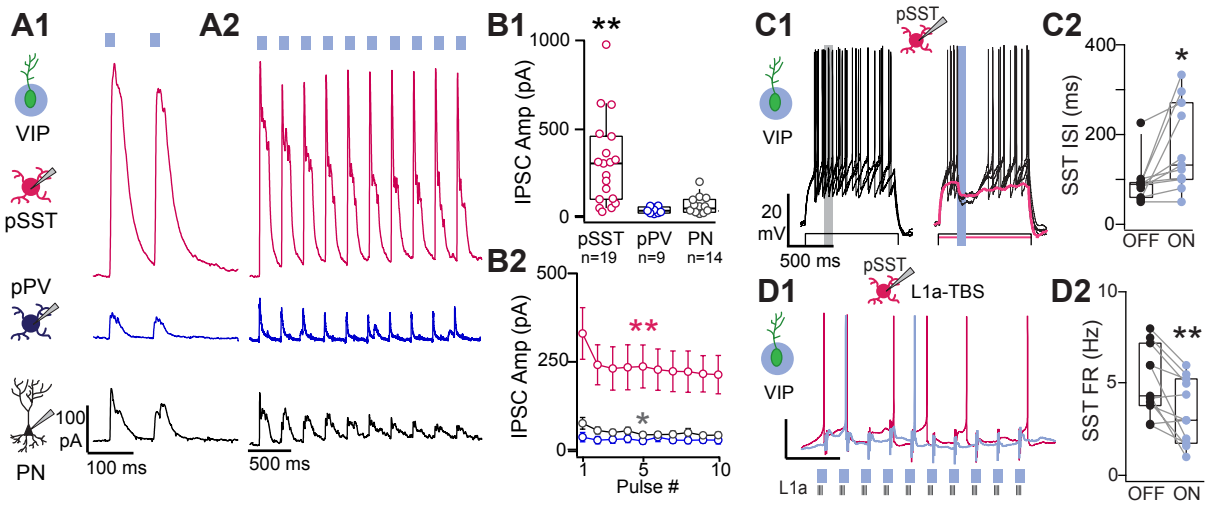


**Figure 3: Inhibition by VIP-interneurons in piriform cortex.** A1) VIP-INs express ChR2. Optically evoked IPSCs were recorded in putative(p) pSST-INs (magenta), pPV-INs (blue) and PNs (black). A2) Responses of the same neurons (A1) to ten light pulses (100 ms duration, 4 Hz). B1) IPSC amplitude was stronger in pSST-INs versus pPV-INs (*p:0.014) or PNs (*p:0.042, ANOVA). B2) In pSST-INs, IPSC amplitude diminishes by the 5th pulse of theta stimulation (**p: 0.009, paired t-test). C1) IPSCs from VIP-INs delay pSST-IN spike responses during suprathreshold depolarization (4 overlaid traces) Left: Control, Right: activation of VIP-INs (100 ms pulse, blue). Magenta trace: VIP-IN mediated IPSC during subthreshold depolarization. C2) Interspike interval (ISI) was significantly increased during optical activation of VIP-INs (blue circles, p: 0.016, paired t-test, n=11) compared to light off trials (black circles). D1) Spike responses in pSST-INs during TBS in control (magenta trace) and during pulsed light (blue trace). D2) pSST-IN firing rates decreased during TBS on light trials (blue) versus control (black circles, p:0.002, paired t-test, n=11).

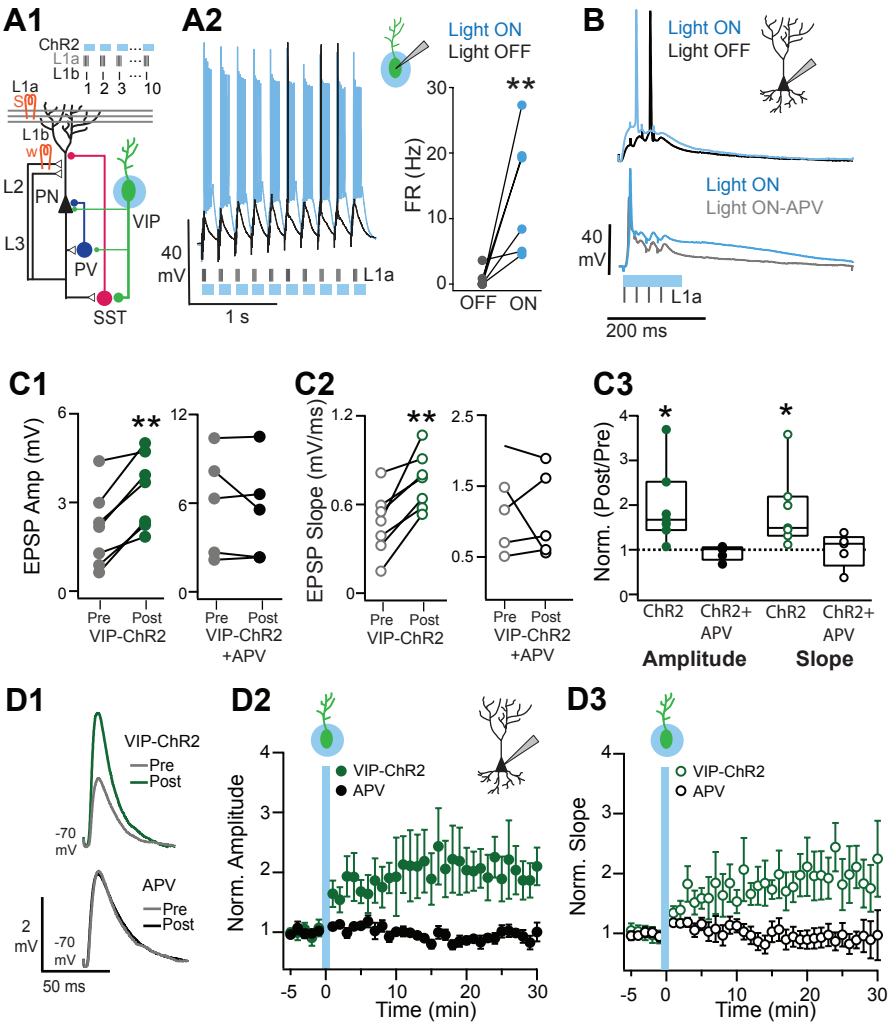


**Figure 5: VIP-interneuron activation promotes associative LTP**. A1) Circuit schematic: VIP-INs express ChR2 and were activated using theta pulsed light during L1a+L1b pairing. A2) VIP-IN responses during TBS without (black) and with light (blue). FRs increase during pairing with light (blue circles, $p<0.05$, WSR, n=7). B) Top: Activation of VIP-INs enhanced PN depolarization during TBS stimulation (blue vs. black trace). Bottom: PN depolarization during VIP-IN activation (blue trace) is reduced by APV (gray trace). C1) Average EPSP amplitude (mV) pre (-5 to 0 min) and post induction (25-30 min) with VIP-IN activation (green) or with VIP-IN activation plus bath application of APV (black). C2) Average slope (mV/ms) of the rising phase of the EPSP pre and post induction, colors as in C1. C3) Normalized EPSP amplitude and slope following pairing with VIP-IN activation (green circles) or with activation plus APV (black). D1) Representative average traces pre (gray) and post induction in with VIP-IN activation (green) or activation plus APV (Black). D2) Time course of normalized EPSP amplitude pre and post induction with activation of VIP-INs (blue box, t=0) in control (green) and with APV (black). D3) Time course of normalized EPSP slope, colors as in D2.